Long-time translational self-diffusion in isotropic dispersions of colloidal rods

M. P. B. van Bruggen,* H. N. W. Lekkerkerker, and J. K. G. Dhont
Van 't Hoff Laboratory for Physical and Colloid Chemistry, Debye Research Institute, Utrecht University, Padualaan 8, 3584 CH Utrecht, The Netherlands
(Received 31 March 1997)

A dispersion of fluorescent colloidal silica coated boehmite rods with length $L \approx 325$ nm and diameter $D \approx 46$ nm, dispersed in dimethylformamide, is synthesized. The concentration dependence of the long-time translational self-diffusion coefficient D_s^L is measured with fluorescence recovery after photobleaching up to a rod volume fraction $\phi = 0.22$. A linear dependence of D_s^L on concentration is found up to $(L/D)\phi = 1$. At higher concentration D_s^L levels off and decreases to 3% of its value at infinite dilution for $(L/D)\phi = 1.5$. [S1063-651X(97)05110-6]

PACS number(s): 82.70.Dd

I. INTRODUCTION

Diffusion of rodlike particles such as the tabacco mosaic virus (TMV) and bacteriophage fd and macromolecules such as poly(γ-benzyl α,L-glutamate) (PBLG) and DNA has been investigated with dynamic light scattering (DLS) [1–5] as well as with forced Rayleigh scattering (FRS) [6] and fluorescence recovery after photobleaching (FRAP) [7,8]. DLS measurements have provided information on diffusion in the limit of infinite dilution and on *collective diffusion* at higher concentrations. With FRS and FRAP information about *long-time self-diffusion* is obtained. With DLS it is difficult to obtain accurate self-diffusion data because for this purpose well-defined tracer systems are required. So far, FRAP and FRS have only been applied to the semiflexible macromolecules DNA [6,7] and PBLG [8]. No long-time self-diffusion data for systems of interacting, rigid rodlike particles have been published in literature to our knowledge.

The aim of this paper is to obtain long-time self-diffusion data with FRAP of rigid colloidal rods. The behavior of the long-time self-diffusion coefficient as concentration increases is relevant for the kinetics of a number of processes such as liquid-crystal phase transitions and gelation, which may occur in dispersions of rodlike particles. Furthermore, the measurements enable us to test theories and computer simulations about self-diffusion properties of rigid rods of well-defined geometry.

For this study we prepared and characterized a system of fluorescent inorganic colloidal rigid rods, consisting of particles with a boehmite (AlOOH) core, surrounded by a shell of silica (SiO_2) in which the fluorescent dye fluorescein isothiocyanate (FITC) is incorporated. These composite particles can be prepared with a variable length and diameter, albeit with a standard deviation of 40% in length and 10% in diameter. The interaction potential between these particles can be varied not only by changing the salt concentration in the dispersion medium, but also by attaching different steric stabilizers to the silica surface. Except for the polydispersity, these features are distinct advantages over the commonly used rigid rodlike colloidal particles such as the TMV.

This paper is organized as follows. Experimental details of the particle preparation and characterization, as well as a description of the interactions involved, are collected in Sec. II. The theory of translational diffusion of rigid rods is surveyed and relevant computer simulation results are summarized in Sec. III. In Sec. IV experimental details of the measurements and the results are given. These results are discussed and compared with theory and simulations in Sec. V. Finally, Sec. VI contains a summary and some concluding remarks.

II. SYSTEM

A. Particle synthesis

An aqueous boehmite (AlOOH) dispersion was prepared according to the method of Buining *et al.* [9]. This starting boehmite dispersion is coded as *B*. The *B* dispersion was subsequently coated with silica in a three-step coating procedure.

The first silica coating procedure is described by Philipse, Nechifor, and Pathmamanoharan [10]. Dispersion *B* is mixed with a solution of sodiumsilicate (Fluka) from which a thin layer of silica deposits on the boehmite rods. This dispersion is coded as BS1. In the next step tetraethoxysilane (Fluka) is emulsified in a alkaline BS1 dispersion. A second layer of silica is deposited on the rods, yielding a dispersion coded as BS2. The silica coating of BS2 is about 2–3 nm thick. To obtain a thicker and also a more smooth coating, BS2 was further grown in a modified Stöber [11] mixture where the rods act as seeds. The resulting dispersion is coded as BS3. The aspect ratio of these rods can be tuned by the total amount of added tetraethoxysilane during the seeding growth.

BS3 was made fluorescent by incorporating FITC (Sigma), following the procedure of van Blaaderen and Vrij [12]. The fluorescent surface was finally covered with silica once more. The dispersion medium was subsequently changed from the water and ethanol mixture to dimethylformamide (DMF) (Baker) by vacuum distillation. As a consequence of the removal of water during the distillation, a large part of the free dye was attached on the particle surfaces. This was concluded from the observation that after sedimentation the supernatant was almost colorless. The fluorescent

*Author to whom correspondence should be addressed.

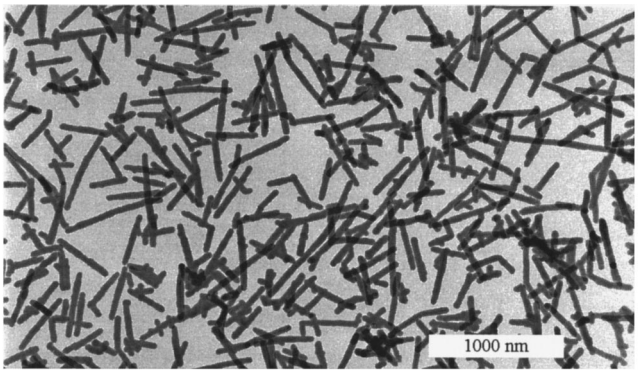

FIG. 1. Transmission electron micrograph of triple silica coated boehmite rods that are labeled with fluorescein isothiocyanate. This system is abbreviated in the main text as BS3F (boehmite, silica, triple coated, fluorescent).

rods therefore do carry dye on their surfaces. The dispersion, coded as BS3F, was further purified through repeated centrifugation at 2500 rpm. A more detailed description of the synthesis will be discussed elsewhere.

Because only a small amount of BS3F was available, no accurate mass density measurement of the rods could be performed. Instead the rod density (ρ_r) was calculated by taking the volume averaged density

$$\rho_r = \frac{\langle V_r \rangle - \langle V_b \rangle}{\langle V_r \rangle} \rho_s + \frac{\langle V_b \rangle}{\langle V_r \rangle} \rho_b \tag{2.1}$$

using literature values for the density of boehmite ($\rho_b = 3.0\ \mathrm{g\ cm^{-3}}$ [13]) and the density of Stöber silica ($\rho_s = 1.78\ \mathrm{g\ cm^{-3}}$ [14]). $\langle V_r \rangle$ is the average volume of the BS3F rods and $\langle V_b \rangle$ the average volume of the boehmite cores. The rods were assumed to be cylindrical so that their average volume is given by $\pi/4\langle D^2 \rangle \langle L \rangle$, with D the diameter of the rods and L their length. L and D were measured from several electron transmission micrographs with use of an interactive image analysis computer program, as described in the following subsection.

B. Particle characterization

Because all measurements are performed with BS3F we will mainly focus on this system. The rods in the starting B dispersion had an average length of 250 nm and width of 10 nm. The polydispersity σ_x, defined as $[\langle x^2 \rangle / \langle x \rangle^2 - 1]^{1/2}$, was about 30% in both dimensions. An electron transmission micrograph of the BS3F dispersion is shown in Fig. 1. From five of these micrographs the average length and width of the rods was determined. For the average length, 760 particles were measured, whereas for the width 310 particles were sufficient to obtain a good average since the polydispersity in width was much smaller than the polydispersity in length. The results and size distributions are given in Table I and Figs. 2(a) and 2(b). Compared to the original B dispersion, the polydispersity in length unfortunately increased to 41%. This fact, in combination with the shape of the length distribution in Fig. 2(b), indicates that during the silica coating procedures some head-to-tail aggregation has taken place. As a consequence, the average length has increased more than the average thickness. This type of aggregation has also been observed in other dispersions of rodlike particles [15]. It also explains the long tail at the right of the maximum of the size distribution in Fig. 2(b). On the other hand, the polydispersity in width significantly decreased to 10%. The width distribution resembles a Gaussian. From the average dimensions of the rods, the average aspect (length to diameter) ratio is found to be 7.1. The volume-averaged density of the particles was calculated from the literature values of boehmite and Stöber silica and is found to be $1.84\ \mathrm{g\ cm^{-3}}$. In addition to size polydispersity, there is to a certain extent some shape polydispersity in the system, meaning that there are also some doublets (crosses) and other small clusters present.

TABLE I. Average dimensions of the BS3F particles as determined by interactive image analysis.

	Width (nm)	Length (nm)
mean	46	323
median	45	299
standard deviation	5	133

C. Interactions

For a dispersion of charge-stabilized, uniform, and rigid colloidal rods, the interaction potential can be described by the classical Derjaguin-Landau-Verwey-Overbeek (DLVO)

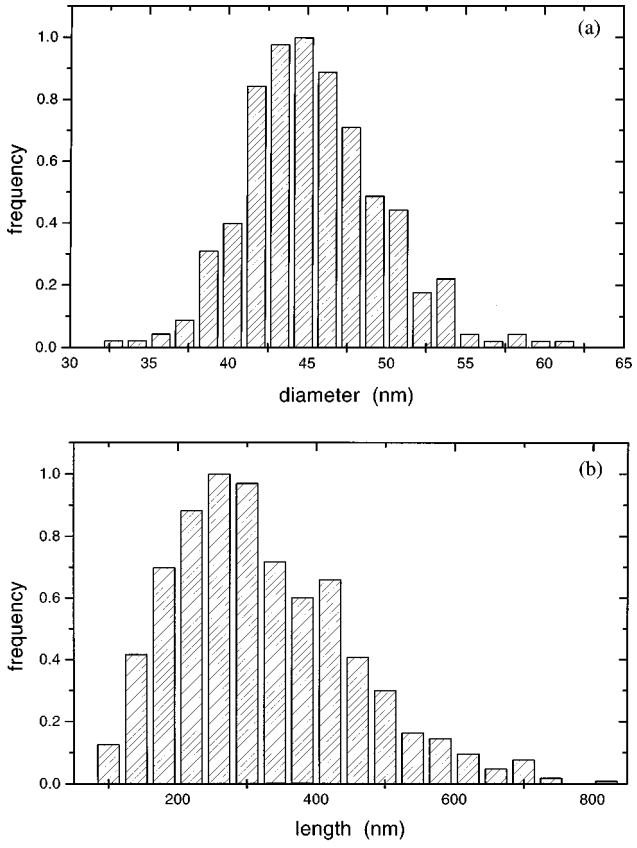

FIG. 2. (a) Diameter distribution of BS3F as determined by interactive image analysis. (b) Length distribution of BS3F as determined by interactive image analysis.

theory. The potential (free) energy V between two rods is the sum of the van der Waals attraction V_A and the double-layer repulsion V_R:

$$V(\hat{\mathbf{u}}_1,\hat{\mathbf{u}}_2,\hat{\mathbf{R}}_{1,2}) = V_A(\hat{\mathbf{u}}_1,\hat{\mathbf{u}}_2,\hat{\mathbf{R}}_{1,2}) + V_R(\hat{\mathbf{u}}_1,\hat{\mathbf{u}}_2,\hat{\mathbf{R}}_{1,2}). \tag{2.2}$$

For rods V is not only a function of the distance between the centers of mass $R_{1,2}$ but is also a function of their mutual orientation $\hat{\mathbf{u}}_1$, $\hat{\mathbf{u}}_2$, and their orientation with respect to $\hat{\mathbf{R}}_{1,2}$.

The *range* of the double-layer repulsion is determined by the screening length (Debye length) κ^{-1}:

$$\kappa^{-1} = \left(\frac{\varepsilon_0 \varepsilon_r RT}{F^2 \Sigma_i c_i z_i^2} \right)^{1/2}, \tag{2.3}$$

with ε_0 the dielectric constant in vacuum, ε_r the relative dielectric constant of the solvent, R the gas constant, T the absolute temperature, F Faraday's constant, and c_i the molar concentration of ions of type i with valence z_i. The *strength* of the van der Waals attraction is determined by the Hamaker constant A of two rods, interacting through a medium. This constant is tabulated for only a few solids in commonly used solvents. The Hamaker constant can also approximately be expressed [16] in terms of the static dielectric constant of the medium and particle ε_m and ε_p and their refractive indices in the visible n_m and n_p:

$$A = \frac{3}{4} k_B T \left(\frac{\varepsilon_p - \varepsilon_m}{\varepsilon_p + \varepsilon_m} \right)^2 + \frac{3h\langle v_e \rangle}{16\sqrt{2}} \frac{(n_p^2 - n_m^2)^2}{(n_p^2 + n_m^2)^{3/2}}, \tag{2.4}$$

with k_B Boltzmann's constant, T the absolute temperature, h Planck's constant, and $\langle v_e \rangle$ the mean electronic vibration frequency of the rods and the medium.

V can be calculated analytically for crossed and parallel orientation under the constraint that $\hat{\mathbf{u}}_1 \cdot \hat{\mathbf{R}}_{1,2} = \hat{\mathbf{u}}_2 \cdot \hat{\mathbf{R}}_{1,2} = 0$. The rather long expressions for V_R and V_A are given in Ref. [17].

With respect to colloidal stability DMF is a convenient solvent. First, the refractive index of DMF (1.43) is close to the refractive index of silica (1.45) so that the Hamaker constant is small. Another special feature of DMF is that it tends to solvate silica [18]. Disrupting this solvation shell costs enthalpy, giving rise to an increase of the total free interaction energy as particles closely approach [19]. The DLVO potential in Eq. (2.2) should therefore also contain a short-range repulsion term that takes this effect into account. Indeed, the particles in BS3F were stable in 0.01M LiCI. Between crossed polarizers the dispersion became birefringent when stirred. Moreover, the dispersion was easily redispersed after prolonged centrifugation at 2500 rpm.

D. Phase behavior

Repulsive, rodlike colloidal particles and polymers are expected to separate into a liquid crystalline and isotropic phase at sufficiently high volume fractions. The theory for this entropy-driven phase separation of rods with hard-core interactions has already been formulated by Onsager [20]. For example, isotropic-nematic phase separations in dispersions of sterically stabilized dispersions of boehmite rods in cyclohexane have been observed [21,22]. Charge-stabilized rods also separate into two phases, although at much lower volume fractions as compared to hard rods [23,24]. An important reason for this is that charge-stabilized colloids have a larger effective excluded volume. The ''effective'' excluded volume may be obtained from Sparnaay's equations for the double-layer repulsion [17], by replacing the diameter D of the rods by an effective diameter D_{eff}, which can be given as

$$D_{\text{eff}} = D + \kappa^{-1} \ln\left[64 \sqrt{\frac{\pi}{2}} c N_{\text{Av}} \tanh^2\left(\frac{F|\phi_0|}{4RT} \right) D^{1/2} L \kappa^{-3/2} \right], \tag{2.5}$$

with c the molar salt concentration (per m^3), N_{Av} Avogadro's constant, and $|\varphi_0|$ the absolute surface potential. D_{eff} corresponds to the rod-rod distance at which the DLVO potential for two *parallel* rods is $1 k_B T$ per rod. van der Waals attraction is neglected in this expression. Since a 0.01M LiCl solution in DMF is only dissociated for 88% [19], $\kappa^{-1} = 2.2$ nm. The surface potential of silica spheres in 0.01M LiCl in DMF is found to be -49 mV [19]. Substituting all relevant parameters yields

$$D_{\text{eff}} = D + 6.4\kappa^{-1}. \tag{2.6}$$

At this distance the van der Waals attraction is less than 1% of the double-layer repulsion. We remark that the D_{eff} as given by Eq. (2.5) is an approximation since no orientational averaging is performed. Because the double-layer repulsion of two rods in a head-tail conformation is much shorter ranged than for parallel orientation, it is justified to take $L_{\text{eff}} \approx L$. The increased excluded volume is opposed by the so-called twist effect; rods tend to lower their interaction free energy by adopting crosslike structures. A measure for this tendency is expressed by the twist parameter h, which is given by [25]

$$h = \frac{\kappa^{-1}}{D_{\text{eff}}} \tag{2.7}$$

and is only 0.037 in this case, indicating that twist effects are not important for these thick rods. According to Onsager's theory for hard rods with a diameter as given by Eq. (2.6), the volume fraction where the isotropic-nematic phase transition occurs is equal to 35%. However, the facts that the rods are not monodisperse and also have a finite aspect ratio both lead to a *decrease* of this volume fraction [26,27].

In the samples under investigation with a volume fraction up to 22%, no phase separation was observed over periods of several weeks. However, in the bottom of the tube of a sample with an initial homogeneous concentration of 22%, small nematic droplets (tactoids) became visible under the polarization microscope after about 4 weeks. In Fig. 3 a polarization light micrograph of the birefringent droplets is shown. It appears that tactoid formation takes place when due to sedimentation a threshold concentration in the sediment is reached. The slow appearance of the tactoids might be explained by the fact that sedimentation is a slow process in the systems considered here. But also the growth of the droplets to sizes visible in the microscope may be slow as well. From the work of Philipse [28] it is known that for

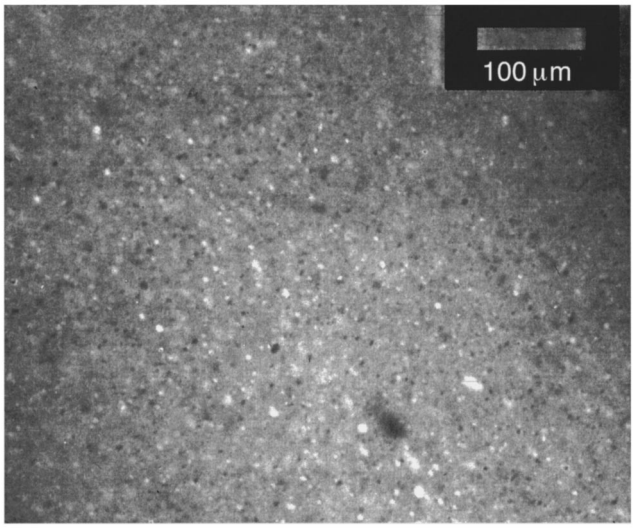

FIG. 3. Polarization light micrograph between crossed polarizers of the sediment of BS3F with an overall volume fraction of 22%. Due to sedimentation the rod concentration on the bottom of the cuvette increases and above the isotropic-nematic phase boundary small nematic droplets (tactoids) become visible. These droplets appear as dark or bright spots on the micrograph.

particles with an aspect ratio of 7 the maximum random packing fraction is about 30%, so the volume fraction in the sediment is not expected to exceed 30%. The isotropic-nematic phase boundary is therefore expected to be situated somewhere between 22% and 30%. This is in agreement with the theoretical prediction. As will become clear in Sec. IV, at this volume fraction the rods diffusivity is strongly retarded, which might give rise to the slow phase separation kinetics as observed.

III. TRANSLATIONAL SELF-DIFFUSION

A. Translational diffusion at infinite dilution

The translational diffusion coefficient D of a Brownian rod in the isotropic phase is the orientational average of the diffusion coefficients parallel and perpendicular to the rods long axis, $D_{\parallel}$ and $D_{\perp}$,

$$D=\tfrac{1}{3}D_{\parallel}+\tfrac{2}{3}D_{\perp}, \tag{3.1}$$

for all volume fractions ϕ. In the limit of infinite dilution the rods move without interacting with other rods and only experience a hydrodynamic friction with the solvent. In this case $D_{\parallel}$ and $D_{\perp}$, now denoted as $D_{0,\parallel}$ and $D_{0,\perp}$, are given by

$$D_{0,\parallel}=\frac{k_BT}{2\pi\eta_mL}\left[\ln\left(\frac{L}{D}\right)-0.207+0.980\,\frac{D}{L}-0.133\left(\frac{D}{L}\right)^2\right],$$

$$\phi\to 0, \tag{3.2a}$$

and

$$D_{0,\perp}=\frac{k_BT}{4\pi\eta_mL}\left[\ln\left(\frac{L}{D}\right)+0.839+0.185\,\frac{D}{L}+0.233\left(\frac{D}{L}\right)^2\right],\quad \phi\to 0, \tag{3.2b}$$

with η_m the viscosity of the medium, L the length of the rod and D its diameter, k_B Boltzmann's constant, and T the absolute temperature. The last three terms within the square brackets in Eqs. (3.2a) and (3.2b) are corrections to take end effects into account. Here we used the corrections proposed by Tirado, Martinez, and de la Torre [29]. Combining Eqs. (3.1), (3.2a), and (3.2b) yields

$$D_0=\frac{k_BT}{3\pi\eta_mL}\left[\ln\left(\frac{L}{D}\right)+0.316+0.5825\,\frac{D}{L}+0.050\left(\frac{D}{L}\right)^2\right],\quad \phi\to 0. \tag{3.3}$$

As concentration increases the particles will start to interact and the translational diffusion coefficient will become a function of concentration.

B. Concentration dependence of the translational diffusion coefficient

It is customary to distinguish three concentration regimes [30]: the dilute regime where the rod volume fraction ϕ is equal to or smaller than $(D/L)^2$, the semidilute regime in the range $(D/L)^2\ll\phi\ll D/L$, and the concentrated regime where ϕ is equal to or larger than D/L. In all these three regimes one must distinguish between short- and long-time self-diffusion. With FRAP one probes the long-time self-diffusivity of colloidal dispersions and therefore in the following we will focus only on this type of diffusion.

In the *tube model* of Doi and Edwards [31] the rods lose the ability to move perpendicular to their long axis at higher concentration, while diffusion parallel to the long axis remains equal to $D_{0,\parallel}$. This is reasonable in the semidilute regime for rods with a large aspect ratio. Following this line of reasoning Edwards and Evans [32] developed a Green's function formalism to calculate the concentration dependence of $D_{\parallel}$ at concentrations around D/L. This work was extended to even higher concentrations by Sato and Teramoto [33]. The same formalism was used by Teraoka and Hayakawa [34] to describe the concentration dependence of $D_{\perp}$ in the dilute and semidilute regimes. Recently, Szamel [35] proposed yet a different approach based on the Smoluchowski equation and derived a similar expression for $D_{\perp}$ in the dilute and semidilute regimes. Note that in the above-mentioned theoretical work either $D_{\parallel}$ or $D_{\perp}$ is explicitly evaluated; in the semidilute regime one always assumes that $D_{\parallel}=D_{0,\parallel}$ whereas at higher concentration it is assumes that $D_{\perp}=0$. In this paper the concentration regimes of interest are the dilute and semidilute. However, there is no theory that predicts how $D_{\parallel}$ depends on concentration in this range of concentrations. To obtain a rough estimate for the concentration dependence of the long-time self-diffusion coefficient D_s^L within the experimental range of concentrations, let us assume that for concentrations smaller than $(D/L)^2$, $D_{\parallel}$ may

be set equal to $D_{0,\parallel}$. If we now use the expression for $D_\perp(\phi)$ as derived by Teraoka and Hayakawa [34],

$$\frac{D_\perp(\phi)}{D_{0,\perp}}=\left[1+\gamma^{-1/2}4\pi^{-1}\left(\frac{L}{D}\right)^2\phi\right]^{-2},\quad 0\leqslant\phi\ll\frac{D}{L}, \tag{3.4}$$

with $\gamma^{-1/2}$ a numerical, theoretical unknown constant, and linearize Eq. (3.4) up to first order in ϕ we finally obtain, after orientational averaging,

$$\frac{D_s^L(\phi)}{D_0}=1-\frac{\frac{4}{3}D_{0,\perp}}{D_0}\,\gamma^{-1/2}4\pi^{-1}\left(\frac{L}{D}\right)^2\phi,\quad 0\leqslant\phi<\left(\frac{D}{L}\right)^2. \tag{3.5}$$

Note that the product $4\pi^{-1}(L/D)^2\phi$ is equal to the number of rods in a volume L^3 with L the length of the rods. If the same procedure is performed with the expression for $D_\perp(\phi)$ as derived by Szamel [35],

$$\frac{D_\perp(\phi)}{D_{0,\perp}}=\frac{1}{1+\sqrt{D_{0,\perp}/D_{0,\parallel}}4\pi^{-1}\left(\frac{L}{D}\right)^2\phi F(D_{0,\perp}/D_{0,\parallel})},\qquad 0\leqslant\phi<\left(\frac{D}{L}\right)^2, \tag{3.6}$$

with $F(D_{0,\perp}/D_{0,\parallel})$ a monotonic function changing between $F(0)=0.133$ and $F(1)=0.081$, we find to first order in ϕ

$$\frac{D_s^L(\phi)}{D_0}=1-\frac{\frac{2}{3}D_{0,\perp}}{D_0}\,\sqrt{\frac{D_{0,\perp}}{D_{0,\parallel}}}\,F\left(\frac{D_{0,\perp}}{D_{0,\parallel}}\right)4\pi^{-1}\left(\frac{L}{D}\right)^2\phi,\qquad 0\leqslant\phi\ll\left(\frac{D}{L}\right)^2, \tag{3.7}$$

where $F(D_{0,\perp}/D_{0,\parallel})\approx 0.1$. We remark that Eqs. (3.5) and (3.7) are approximate expressions that are expected to hold only if the rods are much longer than their diameter. Unfortunately, there is no exact low concentration expansion of D_s^L for rodlike particles as has been derived for spherical particles [36,37].

A different approach is proposed by Odijk [38], who calculated the friction factor for a test rod diffusing through an *effective* medium. The effective medium consists of the solvent plus all other rods. These rods are much larger than the test rod so that they diffuse very slowly compared to the test rod. It is assumed that only hydrodynamic interactions with the effective medium influence the long-time self-diffusion of the test rod. Under these assumptions D_s^L can be calculated from the Stokes-Einstein relation $D_s^L=k_BT/f(\xi)$, where the friction factor $f(\xi)$ is given by

$$f(\xi)=\frac{3\pi\eta L}{\ln\left(\frac{\xi}{a}\right)+\ln 2-\gamma}, \tag{3.8}$$

with L the rod length, η the viscosity of the pure solvent, γ the Euler constant (0.577 22), and ξ a screening length. The screening length is calculated by solving the equation

$$\left(\frac{a}{\xi}\right)^2 K_0\left(\frac{a}{\xi}\right)=3\phi, \tag{3.9}$$

with $K_0(a/\xi)$ the zeroth-order Bessel function and a the rod radius. The range of validity of Odijk's theory is limited to $1\ll\xi/a\ll L/a$. For small aspect ratios Eq. (3.9) is therefore valid only within a small range of concentrations.

C. Computer simulations

Molecular-dynamics, Brownian dynamics (BD), and Monte Carlo (MC) simulations have been used for the calculation of the concentration dependence of the long-time self-diffusion coefficient D_s^L. Initial computer simulations in this area were performed by Frenkel and Maguire [39] on Newtonian rods that are infinitely thin. These simulations were extended to higher concentrations by Magda, Davis, and Tirrell [40]. Doi, Yamamoto, and Kano [41] performed MC simulations, again considering infinitely thin rods but also including a stochastic noise to incorporate Brownian motion. In this simulation D/D_0 falls to 0.5 in the concentrated regime, resembling the prediction of the original Doi-Edwards theory. In recent years more realistic simulations have been published on Brownian rods with finite thickness [42,43]. Löwen [44] performed BD simulations on hard spherocylinders with various aspect ratios up to $L/D=6$. Branka and Heyes [45] performed BD simulations, using a two-site Yukawa potential to include effects of charges. These calculations have been extended recently by Kirchhoff, Löwen, and Klein [46] to a multisegmented Yukawa potential with large Debye lengths. In all simulations mentioned, hydrodynamic interactions were neglected.

IV. MEASUREMENTS

A. Fluorescence recovery after photobleaching

1. Theory

When a laser of sufficiently high intensity is directed on a dispersion of fluorescently labeled particles, the dye molecules within the spot will be bleached irreversibly. This will leave a dark spot in the dispersion. After bleaching, fluorescent particles will diffuse into the spot and bleached particles will leave the spot, causing the fluorescent intensity to recover in time. If particle interactions are not changed due to the bleach process, the recovery of the fluorescence provides information about self-diffusion of the particles.

In the present FRAP setup, instead of a simple spot, a fringe pattern is bleached [47,48]. The fringe pattern is produced by two interfering laser beams that intersect in the dispersion at an angle θ. The wave vector associated with the fringe pattern is equal to

$$K=\frac{4\pi}{\lambda}\sin\left(\frac{\theta}{2}\right), \tag{4.1}$$

where λ is the wavelength of the light in vacuum. Note that the wave vector K in a FRAP experiment does not contain the refractive index of the solvent. The wavelength of the sinusoidal bleach pattern, which will be referred to as the fringe spacing, is equal to $2\pi/K$. After bleaching, the sinusoidal bleach pattern is monitored with the same fringe pat-

tern with reduced intensity. It oscillates between two adjacent extrema of the bleach pattern with a known frequency of typically 1 kHz. An oscillating fluorescent intensity with a diminishing amplitude is detected. Hence, contrary to the original FRAP setups where a spot is bleached, not a *recovery* but rather a *decay* of the FRAP signal is measured. Technical details about the FRAP setup as used in this study are given in Ref. [19].

The fringe pattern remains sinusoidal in time with the same fringe spacing. This is a consequence of Fick's diffusion equation

$$\frac{\partial}{\partial t}\, c(r,t) = D_s^L \nabla^2 c(r,t), \tag{4.2}$$

with $c(r,t)$ the concentration of bleached (or unbleached) particles at time t and position r, which can be written as

$$c(r,t) \propto S(t)\sin(\mathbf{K}\cdot\mathbf{r}), \tag{4.3}$$

where $S(t)$ is the time-dependent amplitude of the fringe pattern. Substituting Eq. (4.3) into Eq. (4.2) then yields

$$\frac{\partial}{\partial t}\, S(t) = -D_s^L K^2 S(t). \tag{4.4}$$

From Eq. (4.4) it follows that the amplitude $S(t)$ of the monitored intensity decays exponentially in time,

$$S(t) \propto \exp(-K^2 D_s^L t). \tag{4.5}$$

At sufficiently small values of θ and consequently for fringe spacings much larger than the particle's size, $-d\ \ln S(t)/dK^2 t$ should be constant and equal to D_s^L. A formal derivation of Eq. (4.5) is found in Ref. [49].

2. Results

BS3F samples were transferred into long thin glass cuvettes (Vitrodynamics Inc.) with a pathlength of 100 μm and a width of 1 or 2 mm. The blue line (488 nm) of an argon-ion laser (Spectra Physics 2000) was used. To prevent heat formation, the reading (I_r) and bleaching beam (I_b) intensities were attenuated with filters such that $I_0/I_b \approx 10$ and $I_0/I_r \approx 100$, with I_0 ($=300$ mW) the laser intensity. The samples were first prebleached at *reading* beam intensity. A typical bleach curve at reading intensity is given in Fig. 4. The curve in Fig. 4 is highly nonexponential, showing that there is a strongly varying bleachability of the various dye molecules in a single colloidal particle. After 300–400 s the most easily bleachable dye molecules are destroyed, after which the decrease over a time lapse of one measuring period, about 1 min, is only a few percent. This indicates the necessity of prebleaching and furthermore it shows that 300–400 s is enough to overcome significant bleaching during the reading period. For each sample 10–20 decay curves were measured, one of which is given in Fig. 5. The decay exponent $\tau(K)$ was obtained by fitting the decay curve to a single exponential $\sim\exp[-\tau(K)t]$. No second cumulant had to be taken into account for obtaining good fits, in contrast to the DLS decay curves, which will be discussed in Sec. IV B. The error in D_s^L was determined by calculating the standard deviation of the series. To check whether indeed self-diffusion was measured, decay curves of one sample, measured at different K values, were gathered. In Fig. 6 the decay exponent is plotted as a function of the squared scattering vector. The linear dependence indicates that indeed long-time self-diffusion is monitored.

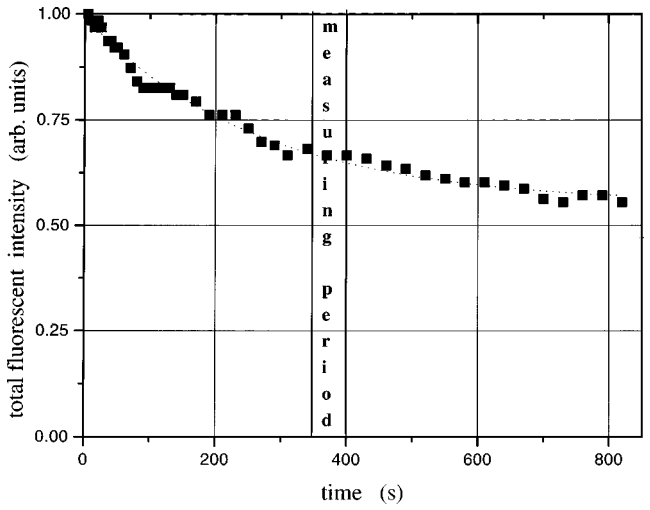

FIG. 4. Bleach curve of a BS3F sample at reading intensity. The detected intensity is the *total* fluorescent intensity. The dotted line is drawn to guide the eye. During the first few minutes significant bleaching occurs at reading intensity, showing the necessity of prebleaching.

Measurements were done on a 0.01M LiCl BS3F dispersion in DMF of high concentration, which was subsequently diluted with a 0.01M LiCl DMF stock solution. In this way a volume fraction range from about 25% down to about 0.5% was covered. The fringe spacing varied from 10.7 μm for the highest volume fractions to 32.6 μm for the lowest volume fractions. Particle volume fractions were determined by measuring the dry weight of a small known amount of dispersion.

The measured long-time translation self-diffusion coefficient D_s^L as a function of the volume fraction ϕ is given in Fig. 7. D_0 was extracted by extrapolation to $\phi = 0$ from the first eight data points, yielding a D_0 of $(19.0 \pm 0.4) \times 10^{-13}$ m^2 s^{-1}. Notice that D_s^L is linear in the volume frac-

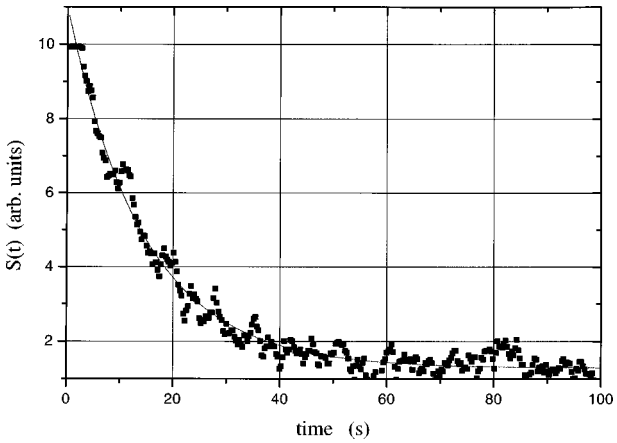

FIG. 5. Typical FRAP curve. $S(t)$ is the amplitude of the fringe pattern that decays in time according to Eq. (4.5). The solid line is a fitted single exponential curve.

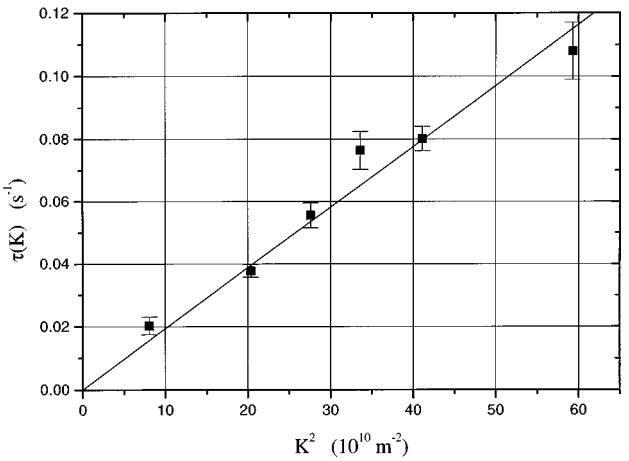

FIG. 6. Fitted decay exponent $\tau(K)$, as determined from the FRAP curves, versus the wave vector K squared. The linear dependence indicates that indeed the long-time limit is monitored in this range of K's. The drawn line is a linear fit through the origin.

tion ϕ up to about 15%, corresponding to $(L/D)\phi \approx 1$. Such a remarkable linear decrease of D_s^L over a large range of concentrations is also observed for spheres [19,49]. For $(L/D)\phi > 1$, D_s^L levels off to about 3% of its value D_0 at infinite dilution.

B. Dynamic light scattering

1. Theory

In a dynamic light scattering experiment one measures, as a function of the scattering angle, the autocorrelation function of the scattered intensity. The Siegert relation relates the intensity autocorrelation function (IACF) to the field autocorrelation function (EACF) as

$$\hat{g}_1(K,t) = 1 + |\hat{g}_E(K,t)|^2, \tag{4.6}$$

where $\hat{g}_E(K,t)$ is the normalized EACF and $\hat{g}_I(K,t)$ the normalized IACF. The decay of the normalized IACF contains

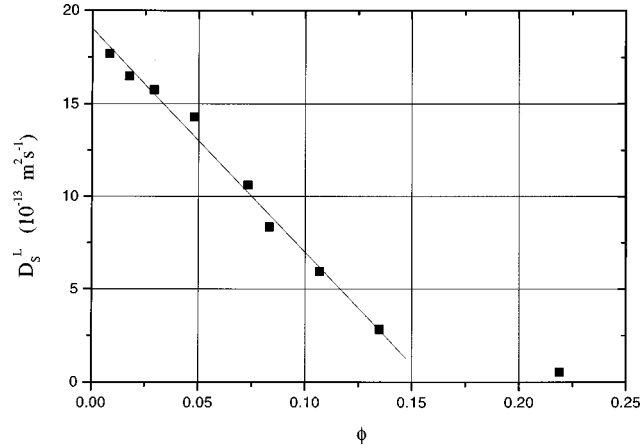

FIG. 7. Measured long-time translational self-diffusion coefficient D_s^L as a function of the volume fraction ϕ. The error in the measured diffusion coefficient is about 10%. The linear dependence between D_s^L holds up to a volume fraction of about 15% or, equivalently, up to $(L/D)\phi = 1$. The solid line is a linear fit.

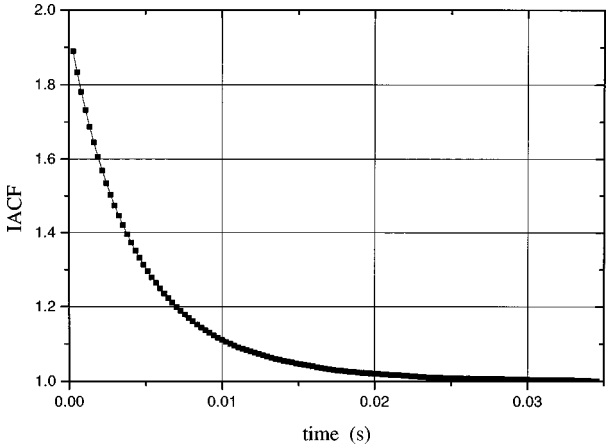

FIG. 8. Intensity autocorrelation function (IACF) as a function of time for $KL = 2.70$, measured in a BS3F sample with $\phi \approx 0.002$.

information about the translational and the rotational diffusivity of the rods. For a very dilute dispersion of rods the normalized EACF can be expanded in a series of exponents [50]

$$\begin{aligned}\hat{g}_E(K,t) = \exp\{-K^2 t[C(KL)\Delta D + D_0]\} \\ \times [S_0(KL) + S_2(KL)\exp(-6D_{0,r}t) \\ + S_4(KL)\exp(-20D_{0,r}t) + \cdots],\end{aligned} \tag{4.7}$$

where the ''coupling function'' $C(KL)$ represents the coupling between rotational and translational diffusion, $\Delta D = D_{0,\parallel} - D_{0,\perp}$, D_0 is the translational diffusion coefficient, and $D_{0,r}$ is the rotational diffusion coefficient, both at infinite dilution. The prefactors $S_{2n}(KL)$ with $n > 0$ and the coupling function $C(KL)$ both complicate the analysis of the IACF. However, for $KL < 5$, both the coupling between rotation and translation and the coefficients S_{2n} for $n > 0$ may be neglected [50]. Since for $KL < 5$, $S_0(KL)$ is almost unity, the Siegert relation reads

$$\hat{g}_1(K,t) \approx 1 + \exp(-2K^2 D_0 t) \quad \text{for } KL < 5. \tag{4.8}$$

In this wave-vector region only the translational diffusion contributes to the decay of the IACF.

2. Results

D_0 was measured with dynamic light scattering using a sample with a concentration of about 0.1 vol %, corresponding to $(L/D)\phi = 0.007$. We used an argon-krypton laser (Spectra Physics 2020, $\lambda = 647.1$ nm). At this wavelength the dye molecules hardly absorb light [12] so that heating effects are practically absent. Scattering angles ranged from 30° to 120°. The IACF's were fitted to a single exponential, including a second cumulant to account for polydispersity $\alpha + \beta \exp[-b(K)t + c(K)t^2]$, with $b(K)$ the decay exponent and $c(K)$ the second cumulant. A typical IACF together with its fit is given in Fig. 8. The decay exponent $b(K)$ is plotted versus the scattering vector squared K^2 in Fig. 9, where K is equal to

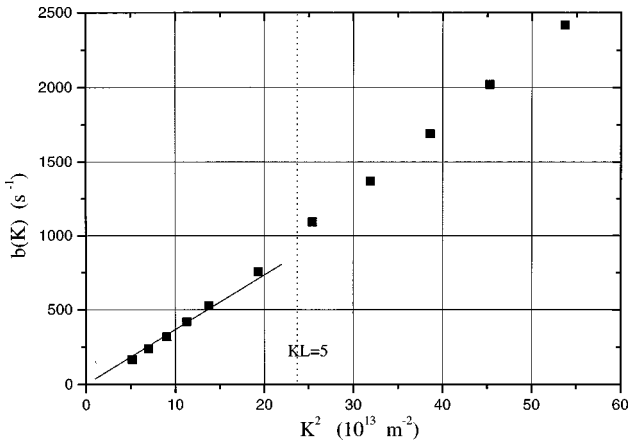

FIG. 9. Fitted decay exponent $b(K)$ of the DLS IACF as a function of the squared wave vector K. The diffusion coefficient at infinite dilution is calculated from the first four points. The vertical dotted line marks the wave vector where $KL=5$.

$$K=\frac{4\pi n_m}{\lambda}\sin\frac{\theta}{2}, \tag{4.9}$$

with n_m the medium refractive index and λ the wavelength of the incident laser beam in vacuum and θ the scattering angle. The deviation from linear dependence at higher values of K^2 is attributed to the gradual appearance of rotation contributions and coupling effects between translational and rotational diffusion. Therefore, D_0 was determined from the slope of part of the curve in Fig. 9 where $KL<3$. In this wave-vector range, according to Eq. (4.6), D_0 is found from the slope of $b(K)$ versus K^2. The translation diffusion coefficient was thus found to be $(18.4\pm0.4)\times10^{-13}$ m^2 s^{-1}, in accordance with the value found from the extrapolated FRAP data.

V. DISCUSSION

A. Comparison of FRAP and DLS results

To within experimental errors the two values found for D_0 from FRAP and DLS experiments agree. In a DLS experiment particles are weighed with their volume squared $\sim L^2D^4$, whereas in a FRAP measurement each particle contribution is proportional to its total fluorescent intensity, roughly $\sim LD$, since a large part of the dye molecules is attached to the silica surface. This implies that FRAP should be less sensitive for polydispersity than DLS. The measurements show that the effect of polydispersity, however, is not significant. To compare the experimentally determined D_0 with Eq. (3.3) using a solvent viscosity $\eta_m=0.867$ mPa s for DMF with 0.01M LiCl [49], a length equal to $L=323$ nm, and a diameter $D=46$ nm, we find D_0 to be 36×10^{-13} m^2 s^{-1}. Part of the difference between the theoretical and experimental value might be due to surface irregularities small on a colloidal scale but large on a molecular scale, which lead to an *increase* of the friction factor and therefore to a *decrease* of D_0. Since in DLS as well as in FRAP large particles contribute stronger to the detected signal, also polydispersity will give rise to a measured D_0 that is lower than the theoretical D_0.

B. Comparison of experimental results with experiments, theory, and computer simulations

Figure 7 shows a linear dependence between D_s^L and the volume fraction ϕ, up to $\phi\approx0.15$, corresponding to $(L/D)\phi=1$. Bu *et al.* [8] performed fluorescence recovery after photobleaching measurements on semiflexible PBLG polymers with different molecular weights. They report a virtually constant D_s^L at concentrations up to $(L/D)\phi=0.8$, followed by a gradual nonlinear decrease. We do not find a plateau up to such high volume fractions. Flexibility of the PBLG polymers probably does play a role here. Wang, Garner, and Yu [6] performed forced Rayleigh scattering experiments with short (150 base pairs in length) DNA fragments that are supposed to be slightly flexible. They found a decay of D_s^L with an exponent of about -0.5 at concentrations *far below* the isotropic-nematic phase boundary. At concentrations smaller than the overlap concentration at $\phi\approx(D/L)^2$, a very weak concentration dependence was found. The FRAP results of Scalettar, Hearst, and Klein [7] found with FRAP on phage λ DNA (about 50 000 base pairs in length) a 50% decrease of D_s^L at a concentration range 42–305 mg/l. From their five data points with relatively large error bars it is hard to say whether or not the decrease is linear. Furthermore, it is noted that the DNA used in this study had a high molecular weight so that flexibility of the DNA definitely influences self-diffusion behavior.

Our data are rather similar to the experimental data found for *hard*, spherical particles for which also a linear decrease of D_s^L is observed over a long range of concentrations [49]. The experimental slope of D_s^L/D_0 versus ϕ for hard spherical particles of -2.0 ± 0.2 is in accordance with the theoretically predicted first-order coefficient of -2.10 in the ϕ expansion of D_s^L [37]. Apparently, for spherical particles higher-order interactions cancel as far as their effect on the long-time self-diffusion coefficient is concerned. At least for the rods with the modest aspect ratio studied in the present paper, the same feature is found. A comparison with a theoretical first-order coefficient cannot be made here since so far this coefficient has not been calculated. For higher aspect ratios this cancellation of higher-order interaction contributions remains an open question.

To compare the FRAP results with the theoretical low concentration expansion, the data are also plotted against $(L/D)^2\phi$, a quantity that is proportional to the number of rods in a volume L^3. Since $\kappa^{-1}\ll L$, this rescaled concentration is nearly independent of the salt concentration (remember that in our system $\kappa^{-1}=2.2$ nm and $L=323$ nm). In Fig. 10 D_s^L versus $(L/D)^2\phi$ is shown. In this figure also the data that result from Odijk's [38] effective-medium theory as well as the BD simulation results of Löwen [44] are plotted. The initial slope of the measured D_s^L divided by the extrapolated D_0 versus $(L/D)^2\phi$ is found to be 0.127 ± 0.004. The theoretically unknown factor $\gamma^{-1/2}$ in our formal low-density expansion of the Teraoka-Hayakawa expression (3.5) is found to be 0.084 ± 0.003, in accordance with $\gamma^{-1/2}=0.071\pm0.028$ found by Bu *et al.* for PBLG with an aspect ratio of 6.9. Their value for $\gamma^{-1/2}$ is obtained by taking the concentration dependence of $D_\parallel$ into account by combining the theoretical expressions of Sato and Teramoto for $D_\parallel(\phi)$ with $D_\perp(\phi)$ as given by Teraoka and Hayakawa. These theories, however,

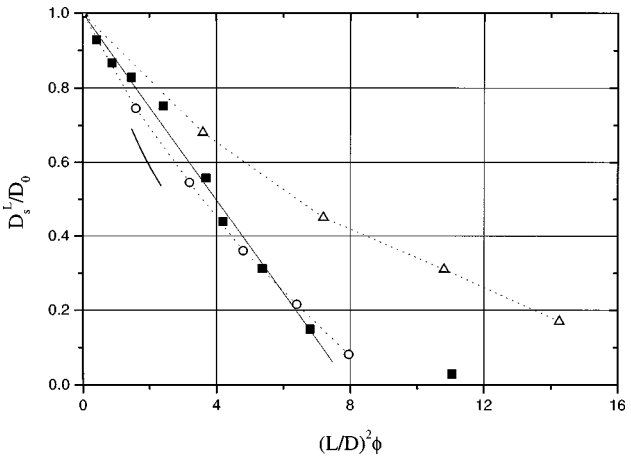

FIG. 10. Measured FRAP data on BS3F indicated by (■), normalized on D_0, as a function of $(L/D)^2\phi$. Note that $(L/D)^2\phi$ is proportional to the number of rods in volume L^3 with L the length of the rods. The BD results of Löwen [44] are given for two aspect ratios $L/D=4$ (○) and $L/D=6$(Δ). The dotted lines are drawn to guide the eye. The prediction of the Odijk theory [38] is given by the solid line without data marks.

are claimed to be valid in different concentration regimes and the agreement between the two numerical values of $\gamma^{-1/2}$ may be fortuitous. In the formal low-density expansion of Szamel's expression, Eq. (3.7), the factor $F(D_{0,\perp}/D_{0,\parallel}=0.749)$ is expected to be 0.1 ± 0.02. This leads to a predicted initial slope of 0.066 ± 0.013, which is twice as low as the experimental slope. Remember that in the derivation of Eq. (3.7) it was assumed that $D_\parallel=D_{0,\parallel}$. Our results clearly indicate that this is not a good assumption for rods with a small aspect ratio. To match the experimental slope, $F(D_{0,\perp}/D_{0,\parallel})$ in Eq.(3.7) should have been 0.192 ± 0.006, which is outside the theoretical domain of $F(D_{0,\perp}/D_{0,\parallel})$ that ranges from 0.081 to 0.133.

Of the several BD simulations reported in literature [42–46], the results of Löwen [44] on *hard* spherocylinders are particularly relevant for comparison with our experimental results. The BD simulations on charged rods [45,46] are less appropriate because of the rod's small aspect ratio in Ref. [45] and the low-salt regime that is focused on in Ref. [46]. In Fig. 10 we display the simulation results of Löwen for $L/D=4$ and 6. Löwen gives an expression for the first order in ϕ coefficient, which is obtained from fits of his simulation data [44]:

$$\frac{D_s^L}{D_0}=1-\left[a_1+a_2\left(\frac{L}{D}-1\right)+a_3\left(\frac{L}{D}-1\right)^2+a_4\left(\frac{L}{D}-1\right)^3\right]\phi, \tag{5.1}$$

with $a_1=1.94$, $a_2=0.310$, $a_3=-0.0569$, and $a_4=0.0151$. Because these simulations are on hard spherocylinders, the aspect ratio of the rods in our system should be corrected for the double-layer repulsion. So instead of the hard-core aspect ratio the effective aspect ratio should be taken: $(L/D)_{\rm eff}\approx L/D_{\rm eff}=5.4$, where $D_{\rm eff}$ is given by Eq. (2.6) as long as $L\gg\kappa^{-1}$. Such a procedure to map the real potential onto a hard-core potential is legitimate in our case where $\kappa^{-1}\ll D$, but certainly fails when κ^{-1} becomes of the order of the diameter of the rods. Substituting $L/D=5.4$ yields a coefficient of -3.49. The experimental slope corresponding to an aspect ratio of 5.4 is equal to -3.71 ± 0.12, which is close to the prediction of Löwen.

In the effective-medium theory of Odijk [38] hydrodynamic interactions are most important, so here it is more appropriate to rely on the rods hard-core aspect ratio of 7.1. The theory overestimates the slowing down of D_s^L with concentration, as can be seen in Fig. 10. Furthermore, we point out that the validity of this theory holds only for the limited range of volume fractions of 2–4 %: The Odijk theory is more appropriate for very long and thin rods.

VI. SUMMARY AND CONCLUSIONS

Colloidal boehmite rods were triple coated with silica and finally covered with a layer of silica in which fluorescein isothiocyanate was incorporated. The rods have a hard-core aspect ratio L/D of 7.1. The polydispersity in length is about 40%, whereas the polydispersity in width is 10%. The particles were dispersed in dimethylformamide and 0.01*M* LiCl was added to screen double-layer repulsion. At a volume fraction between 22% and 30% a nematic phase slowly separated from the isotropic phase. For this model system we were able to measure the concentration dependence of the long-time translational self-diffusion coefficient by using the technique of fluorescence recovery after photobleaching.

The FRAP measurements show a linear dependence of D_s^L with concentration up to $(L/D)\phi\approx1$, resembling the behavior found for hard spheres [19,49] where a linear decrease of D_s^L is observed with a slope that is in accordance with the theoretically predicted first-order coefficient of -2.10 in the ϕ expansion of D_s^L/D_0 [37]. There is no theory yet available for the initial slope of D_s^L/D_0 versus the volume fraction for hard rigid rods. At still higher concentrations D_s^L/D_0 levels off to about 3% at $(L/D)\phi\approx1.5$.

An estimate of the initial slope of D_s^L/D_0 versus the volume fraction for hard rods, based on the results of Szamel [35], underestimates the concentration dependence of D_s^L. From a rough low-density expansion of D_s^L based on the results of Teraoka and Hayakawa [34], a value for the theoretically unknown fit parameter $\gamma^{-1/2}$ is found that closely agrees with the results obtained by Bu *et al.* [8] for semirigid PBLG polymers of similar aspect ratio. The effective-medium theory of Odijk [38], which in fact is more appropriate for rods with large aspect ratios, overestimates the decrease of D_s^L with concentration. The experimental initial slope corresponding to the *effective* hard-core aspect ratio of 5.4 where the aspect ratio is corrected for the double-layer repulsion is found to be -3.71 ± 0.12. This is close to the initial slope of -3.49, as found in Löwen's BD simulations [44] of hard spherocylinders with an aspect ratio of 5.4.

[1] Z. Kam, N. Borochov, and H. Eisenberg, Biopolymers **20**, 2671 (1981).
[2] K. M. Zero and R. Pecora, Macromolecules **15**, 87 (1982).
[3] K. Kubota, H. Urabe, Y. Tominaga, and S. Fujime, Macromolecules **17**, 2096 (1984).
[4] S. Fujime, M. Takasaki-Ohsita, and T. Maeda, Macromolecules **20**, 1292 (1987).
[5] L. M. DeLong and P. S. Russo, Macromolecules **24**, 6139 (1991).
[6] L. Wang, M. M. Garner, and H. Yu, Macromolecules **24**, 2368 (1991).
[7] B. A. Scalettar, J. E. Hearst, and M. P. Klein, Macromolecules **22**, 4550 (1989).
[8] Z. Bu, P. S. Russo, D. L. Tipton, and I. I. Negulescu, Macromolecules **27**, 6871 (1994).
[9] P. A. Buining, C. Pathmamanoharan, J. B. H. Jansen, and H. N. W. Lekkerkerker, J. Am. Ceram. Soc. **74**, 1303 (1991).
[10] A. P. Philipse, A. M. Nechifor, and C. Pathmamanoharan, Langmuir **10**, 4451 (1994).
[11] W. Stöber, A. Fink, and E. Bohn, J. Colloid Interface Sci. **26**, 62 (1968).
[12] A. van Blaaderen and A. Vrij, Langmuir **8**, 2921 (1992).
[13] P. A. Buining, Y. S. J. Veldhuizen, C. Pathmamanoharan, and H. N. W. Lekkerkerker, Colloids Surf. **64**, 47 (1992).
[14] A. van Blaaderen and A. Vrij, J. Colloid Interface Sci. **156**, 1 (1993).
[15] K. Wadu-Mesthrige, B. Pati, W. Martin McClain, and G. Y. Liu, Langmuir **12**, 3511 (1996).
[16] J. N. Israelachvili, *Intermolecular & Surface Forces* (Academic, London, 1991).
[17] M. J. Sparnaay, Recl. Trav. Chim. Pays-Bas. **78**, 680 (1959).
[18] G. P. van der Beek and M. A. Cohen Stuart, Langmuir **7**, 327 (1991).
[19] A. van Blaaderen, J. Peetermans, G. Maret, and J. K. G. Dhont, J. Chem. Phys. **96**, 4591 (1992).
[20] L. Onsager, Ann. (N.Y.) Acad. Sci. **51**, 627 (1949).
[21] P. A. Buining and H. N. W. Lekkerkerker, J. Phys. Chem. **97**, 11 510 (1993).
[22] M. P. B. van Bruggen, F. M. van der Kooij, and H. N. W. Lekkerkerker, J. Phys.: Condens. Matter **8**, 9451 (1996).
[23] H. Zocher, Z. Anorg. Chem. **147**, 91 (1925).
[24] X. M. Dong, T. Kimura, J. F. Revol, and D. G. Gray, Langmuir **12**, 2076 (1996).
[25] A. Stroobants, H. N. W. Lekkerkerker, and T. Odijk, Macromolecules **19**, 2232 (1986).
[26] G. J. Vroege and H. N. W. Lekkerkerker, J. Phys. Chem. **97**, 3601 (1993).
[27] A. R. Khokhlov and A. N. Semenov, J. Stat. Phys. **38**, 161 (1985).
[28] A. P. Philipse, Langmuir **12**, 1127 (1996); **12**, 5971(E) (1996).
[29] M. M. Tirado, C. L. Martinez, and J. G. de la Torre, J. Chem. Phys. **81**, 2047 (1984).
[30] M. Doi and S. F. Edwards, *The Theory of Polymer Dynamics* (Clarendon, Oxford, 1986).
[31] M. Doi and S. F. Edwards, J. Chem. Soc. Faraday Trans. 2 **74**, 560 (1978).
[32] S. F. Edwards and K. E. Evans, J. Chem. Soc. Faraday Trans. 2 **78**, 113 (1982).
[33] T. Sato and A. Teramoto, Macromolecules **24**, 193 (1991).
[34] I. Teraoka and R. Hayakawa, J. Chem. Phys. **89**, 6989 (1988).
[35] G. Szamel, Phys. Rev. Lett. **70**, 3744 (1993).
[36] G. K. Batchelor, J. Fluid Mech. **131**, 155 (1983).
[37] B. Cichocki and B. U. Felderhof, J. Chem. Phys. **89**, 3705 (1988).
[38] T. Odijk, Macromolecules **19**, 2073 (1986).
[39] D. Frenkel and J. F. Maguire, Mol. Phys. **49**, 503 (1983).
[40] J. J. Magda, H. T. Davis, and M. Tirrell, J. Chem. Phys. **85**, 6674 (1986).
[41] M. Doi, I. Yamamoto, and F. Kano, J. Phys. Soc. Jpn. **53**, 3000 (1984).
[42] I. Bitsanis, H. T. Davis, and M. Tirrell, Macromolecules **21**, 2824 (1988).
[43] I. Bitsanis, H. T. Davis, and M. Tirrell, Macromolecules **23**, 1157 (1990).
[44] H. Löwen, Phys. Rev. E **50**, 1232 (1994).
[45] A. C. Brańka and D. M. Heyes, Phys. Rev. E **50**, 4810 (1994).
[46] Th. Kirchhoff, H. Löwen, and R. Klein, Phys. Rev. E **53**, 5011 (1996).
[47] F. Lanni and B. R. Ware, Rev. Sci. Instrum. **53**, 905 (1982).
[48] J. Davoust, P. F. Devaux, and L. Leger, EMBO J. **1**, 1233 (1982).
[49] A. Imhof, A. van Blaaderen, G. Maret, J. Mellema, and J. K. G. Dhont, J. Chem. Phys. **100**, 2170 (1994).
[50] J. K. G. Dhont, *An Introduction to Dynamics of Colloids* (Elsevier, Amsterdam, 1996).